

Analytical polarization curve of DMFC anode

A.A.Kulikovsky ^{*1,2}

¹*Institute of Energy and Climate Research – Electrochemical Process Engineering (IEK-3),
Research Centre Juelich, D-52425 Juelich, Germany*

²*Moscow State University, Research Computing Center, 119991 Moscow, Russia*

(Received January 10, 2013, Revised March 10, 2013, Accepted March 13, 2013)

Abstract. A model for DMFC anode performance is developed. The model takes into account potential-independent methanol adsorption on the catalyst surface, finite rate of proton transport through the anode catalyst layer (ACL), and a potential loss due to methanol transport in the anode backing layer. An approximate analytical half-cell polarization curve is derived and equations for the anode limiting current density are obtained. The polarization curve is fitted to the curves measured by Nordlund and Lindbergh and parameters resulted from the fitting are discussed.

Keywords: DMFC anode; polarization curve; modeling

1. Introduction

A great potential of methanol as a high energy-density feed for fuel cells has been recognized seemingly in the early sixties of the last century. One of the first studies of methanol oxidation reaction (MOR) on a Pt electrode has been performed by Frumkin's colleagues Bagotsky and Vasilyev (1964). A year later, Frumkin's group reported superior performance of Pt--Ru alloys for methanol oxidation (Petry *et al.* 1965). Since that time, experimental study of MOR kinetics has been a subject of numerous works, most of which studied MOR on a well-defined crystalline catalyst surface in contact with the liquid electrolyte (Bagotsky and Vasilyev 1967, Tarasevich *et al.* 1983, Lamy and Leger 1991, Gasteiger *et al.* 1993).

In electrochemical studies, every effort is usually made to eliminate mass transport effects, in order to avoid their influence on reaction kinetics. However, due to sluggish kinetics of MOR, a real DMFC anode requires high catalyst loading, and hence the anode is usually 50 to 100 μm thick. At typical operating currents of 100--300 mA cm^{-2} , such a system exhibits quite a substantial resistivity for proton transport, which strongly affects the anode performance. Large anode thickness together with relatively poor proton conductivity make the distribution of the MOR overpotential and rate strongly nonuniform through the anode depth. This non-uniformity is of large interest, as it changes the anode performance and leads to non-uniform electrode degradation.

*Corresponding author, PhD, DSci (Research Professor), E-mail: A.Kulikovsky@fz-juelich.de

The range of cell currents, in which the proton transport loss in the anode can be ignored is estimated as $j < \sigma_t b / l_t$, where σ_t is the anode proton conductivity, b is the Tafel slope and l_t is the anode thickness (Kulikovsky 2010). With σ_t and b from Table 1 and $l_t = 0.01$ cm (100 μm anode catalyst layer), we get $j < 18$ mA cm⁻². Thus, for the cell operating at 100 mA cm⁻², proton transport in the anode catalyst layer (ACL) strongly affects the anode performance.

Numerical modeling of a stepwise MOR mechanism in a porous DMFC anode has been reported in a number of works assuming uniformity of MOR overpotential in the anode (see Meyers and Newman (2002); Krewer *et al.* (2006) and the references therein). Recently, Arisetty *et al.* (2010) developed a numerical through-plane DMFC model, which coupled detailed multistep description of anodic and cathodic reactions with the two-phase transport of reactants in the anode and cathode backing layers. However, Arisetty *et al.* neglected variation of overpotential and reaction rates through the ACL, i.e., they also implicitly assumed ideal proton conductivity of the layer. Note that the “cost” of the stepwise kinetic model of MOR by Arisetty *et al.* (2010) is four kinetic constants in the equations, which need to be determined by fitting model overpotentials to the experimental half-cell polarization curve.

A similar kinetic model of MOR for the isothermal (Krewer *et al.* 2008) and non-isothermal (Ko *et al.* 2008) DMFC was used to characterize the cells by their polarization and impedance curves. The models ignored finite ionic conductivity of the ACL, thereby ignoring the effects due to non-uniformity of the MOR rate through the electrode depth.

Divisek *et al.* (2003) seemingly took into account the spatial variation of the MOR overpotential; however, they did not present results on the through-plane distribution of the MOR rate. Note that *a priori* it is evident, that time- and space-dependent numerical codes for the distributed MOR kinetics in the electrode would be time-consuming; in addition, such codes would include a number of poorly known rate constants.

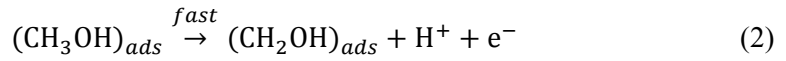
Of large interest is also the nature of the limiting current density j_{lim} in a cell. Typically, a DMFC is run at a high oxygen stoichiometry and relatively low methanol concentration (below 2M), so that the cell limiting current density is determined by the anode side (Scott *et al.* 1999, Baldaus and Preidel 2001, Xu *et al.* 2006). Scott *et al.* (1999) reported proportionality of the limiting current density to the methanol concentration. Xu *et al.* (2006) published a detailed study of the effect of methanol stoichiometry on the limiting current density and analyzed this effect in terms of the mass transfer resistance of the anode side. In their experiments, the limiting current density was also proportional to the methanol concentration and this proportionality was attributed to the methanol transport in the anode backing layer (ABL). Below, we will see that current limitation can be due to the MOR kinetics as well.

Jeng and Chen (2002) developed a numerical through-plane model of DMFC anode with simplified account of the methanol mass transport in the channel. They used Tafel law for the MOR rate, took into account methanol crossover to the cathode and Ohm's law for the proton transport in the CCL. Their model showed large non-uniformity of the MOR rate through the thickness of a 10 μm ACL. However, this work was focused on parametric studies and the effect of the limiting current density has not been studied in detail.

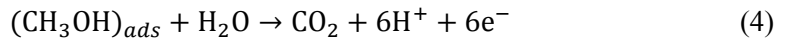
In modeling of cells, stacks and systems, and in design of automatic control devices, a physically realistic analytical equation for the anode polarization curve is highly desirable. Many works utilize the Tafel law for the MOR rate in the electrode (Baxter *et al.* 1999, Dohle *et al.* 2000, Argyropoulos *et al.* 2002, Murgia *et al.* 2003, Yang and Zhao 2007, Casalegno and Marchesi 2008, Miao *et al.* 2008, Cho *et al.* 2009, Zhao *et al.* 2009, Lam *et al.* 2011). This extensive list reflects a great demand for a simple analytical expression for the MOR rate. However, applicability of the

Tafel law to DMFC anode is questionable, as this law neither describes the potential-independent methanol adsorption (see below), nor takes into account the finite rate of proton transport in the electrode.

Jiang and Kucernak (2005) experimentally studied the MOR in a real fuel cell environment, on a Pt/Nafion interface in a porous electrode. According to their work, methanol electro-adsorption on this interface most probably proceeds through a slow step of chemisorption on a Pt surface followed by a fast electrochemical step



Thus, the overall rate of methanol electro-adsorption is determined by the potential-independent chemisorption (1). It is, therefore, reasonable to approximate the MOR kinetics in a DMFC anode by a two-step reaction mechanism



where (4) accumulates all the subsequent electrochemical steps.

Below, we report a one-dimensional through-plane model of a DMFC anode. The model takes into account poor proton transport in the ACL, the two-step kinetics of MOR (3), (4), and the potential loss due to methanol transport in the ABL. The model is solved analytically, and an explicit expression for the half-cell anodic polarization potential is derived. We derive and discuss equations for the limiting current density and show that the finite rate of methanol adsorption on the catalyst surface leads to a specific mechanism of current limitation. The model equation is fitted to the experimental half-cell polarization curves and the fitting parameters are discussed.

This work is an extension of our previous work (Kulikovsky 2003), where a rate expression for MOR similar to that utilized below has been used. However, in (Kulikovsky 2003), this rate expression has not been linked to the reaction scheme (3), (4), which makes it difficult to interpret the results presented there. In addition, the polarization curve in the work discussed has been obtained in the limiting cases of small and large cell current only. Below, a polarization curve which is valid for the whole range of cell currents is derived.

2. Model: basic equations

Consider the anode catalyst layer of a DMFC (Fig. 1). Let the axis x be directed from the membrane to the anode backing layer (ABL). The main model assumption is that the methanol transport in the catalyst layer is fast, i.e., the main contribution to the methanol transport loss is given by the ABL. Physically, methanol transport in the ACL is fast due to the concerted action of diffusion and electroosmotic effect (Jeng and Chen 2002).

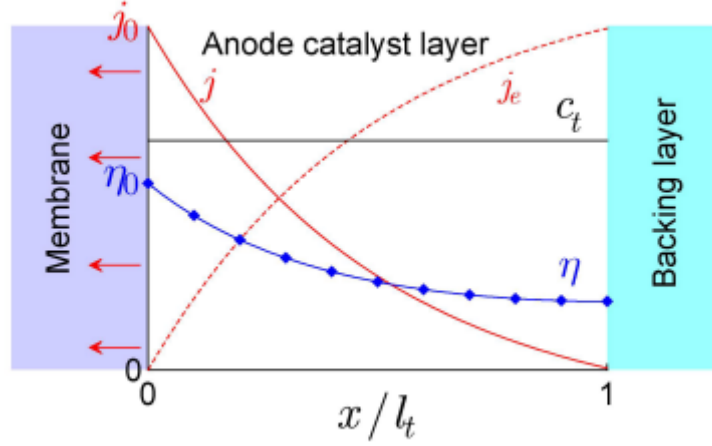


Fig. 1 Schematic of the anode catalyst layer. The proton current density j and MOR overpotential η increase toward the membrane, while the electron current density j_e increases toward the backing layer. The methanol concentration c_t is assumed to be constant along x , though c_t depends of the cell current

The system of equations governing the anode performance is

$$\frac{\partial j}{\partial x} = -R_{MOR} \quad (5)$$

$$R_{MOR} = \frac{i_* \exp(\eta/b)}{1 + i_* \exp(\eta/b)/(i_{ads} c_t / c_{ref})} \quad (6)$$

$$j = -\sigma_t \frac{\partial \eta}{\partial x} \quad (7)$$

where j is the proton current density, η is the MOR polarization voltage (overpotential), c_t , c_{ref} are the methanol concentration in the ACL and the reference concentration, respectively, i_* is the volumetric exchange current density, b is the Tafel slope for MOR, i_{ads} is the volumetric characteristic rate of methanol adsorption on the catalyst surface (A cm^{-3}), and σ_t is the ACL proton conductivity.

Eq. (5) says that the proton current grows toward the membrane due to the proton production in the MOR. The right side of Eq. (5) is a rate of proton production (A cm^{-3}) given by Eq. (6). The latter equation results from the reaction scheme (3),(4)*. Eq. (6) takes into account a zero-order dependence on methanol concentration at low overpotentials and the adsorption step (3). Indeed, as $i_*/i_{ads} \ll 1$ (see below), at small η , the second term in the denominator of (6) is much less

* The prototype of Eq. (6) has been derived by Meyers and Newman (2002); later, similar equation, though with a more complicated concentration dependence was studied by Nordlund and Lindbergh (2004). A simple and transparent derivation of Eq. (6) from the scheme (3), (4) is given in (Kulikovsky 2005).

than unity and this equation reduces to $Q = i_* \exp(\eta/b)$, which is a Tafel law with the zero-order concentration dependence. In the opposite limit of large η , unity in denominator of Eq. (6) can be neglected and this equation reduces to

$$R_{MOR}^{lim} = i_{ads} c_t / c_{ref} \quad (8)$$

which describes the adsorption-limiting rate of MOR. In this regime, the electrochemical conversion steps are fast, and the rate-determining step is a chemisorption process (3). In other words, at high overpotential, the MOR behaves like a “chemical” rather than an electrochemical reaction.

To simplify calculations it is convenient to introduce dimensionless variables

$$\tilde{x} = \frac{x}{l_t}, \quad \tilde{j} = \frac{j}{j_*}, \quad \tilde{\eta} = \frac{\eta}{b}, \quad \tilde{c} = \frac{c}{c_{ref}} \quad (9)$$

where

$$j_* = \frac{\sigma_t b}{l_t} \quad (10)$$

is the characteristic current density. Substituting (6) into (5) and using the variables (9), we get a system of two equations

$$2\varepsilon^2 \frac{\partial \tilde{j}}{\partial \tilde{x}} = - \frac{\exp \tilde{\eta}}{1 + \xi \exp \tilde{\eta}} \quad (11)$$

$$\tilde{j} = - \frac{\partial \tilde{\eta}}{\partial \tilde{x}} \quad (12)$$

where

$$\varepsilon = \sqrt{\frac{\sigma_t b}{2i_* l_t^2}} \quad (13)$$

is the Newman's dimensionless reaction penetration depth, and

$$\xi = \frac{1}{i_{ads} \tilde{c}_t}, \quad \tilde{i}_{ads} = \frac{i_{ads}}{i_*} \quad (14)$$

are the dimensionless parameters. Note that ξ is the inverse characteristic rate of methanol adsorption.

3. Analytical solution

3.1 Through-plane shapes

It is easy to eliminate \tilde{j} from the system (11), (12) by substitution of Eq. (12) into (11). This way, however, leads to a second-order nonlinear equation for $\tilde{\eta}$, which seemingly has no analytical solutions. A better option is to eliminate $\tilde{\eta}$.

Differentiating (11) over \tilde{x} , we get

$$2\varepsilon^2 \frac{\partial^2 \tilde{j}}{\partial \tilde{x}^2} = - \left(\frac{\exp \tilde{\eta}}{1 + \xi \exp \tilde{\eta}} - \xi \left(\frac{\exp \tilde{\eta}}{1 + \xi \exp \tilde{\eta}} \right)^2 \right) \frac{\partial \tilde{\eta}}{\partial \tilde{x}}$$

Taking into account Eqs. (11) and (12), the equation above transforms to

$$\frac{\partial^2 j}{\partial \tilde{x}^2} + \tilde{j} \frac{\partial j}{\partial \tilde{x}} + 2\varepsilon^2 \xi \tilde{j} \left(\frac{\partial j}{\partial \tilde{x}} \right)^2 = 0, \quad \tilde{j}(0) = \tilde{j}_0, \quad \tilde{j}(1) = 0 \quad (15)$$

which contains the proton current density only. The boundary conditions to Eq. (15) are obvious; here \tilde{j}_0 is the cell current density (proton current in the bulk membrane).

It is advisable to rewrite Eq. (15) in the form

$$\frac{\partial^2 j}{\partial \tilde{x}^2} + \tilde{j} \frac{\partial j}{\partial \tilde{x}} \left(1 + 2\varepsilon^2 \xi \frac{\partial j}{\partial \tilde{x}} \right) = 0 \quad (16)$$

In a DMFC anode, parameter $\varepsilon \approx 1 \text{--}10$; however, parameter ξ is typically small: $\xi \sim O(10^{-3})$ (this parameter has been estimated using the data of Nordlund and Lindbergh (2004)). Thus, the product $2\varepsilon^2 \xi \approx 10^{-1} \text{--} 10^{-3}$ and hence at leading order, the term with $\varepsilon^2 \xi$ in Eq. (16) can be omitted (validity of this approximation is discussed in Section 4).

This leads to an equation

$$\frac{\partial^2 \tilde{j}}{\partial \tilde{x}^2} + \tilde{j} \frac{\partial \tilde{j}}{\partial \tilde{x}} = 0 \quad (17)$$

which can easily be integrated to yield (Kulikovsky 2010)

$$\tilde{j} = \gamma \tan \left(\frac{\gamma}{2} (1 - \tilde{x}) \right) \quad (18)$$

Setting in Eq. (18) $\tilde{x} = 0$, we get an equation for parameter γ

$$\tilde{j}_0 = \gamma \tan \left(\frac{\gamma}{2} \right) \quad (19)$$

At small and large \tilde{j}_0 , the solutions to Eq. (19) are (Kulikovsky 2012)

$$\gamma = \begin{cases} \sqrt{2\tilde{j}_0}, & \tilde{j}_0 \ll 1 \\ \frac{\pi \tilde{j}_0}{2 + \tilde{j}_0}, & \tilde{j}_0 \gg 1 \end{cases} \quad (20)$$

The smooth function $\gamma(\tilde{j}_0)$ valid in the whole range of \tilde{j}_0 is (Kulikovsky 2012)

$$\gamma = \frac{\sqrt{2\tilde{j}_0}}{1 + \sqrt{1.12\tilde{j}_0} \exp(\sqrt{2\tilde{j}_0})} + \frac{\pi\tilde{j}_0}{2 + \tilde{j}_0} \quad (21)$$

Note that γ tends to zero as $\tilde{j}_0 \rightarrow 0$.

Eq. (18) with $\gamma(\tilde{j}_0)$ from Eq. (21) gives the leading--order shape of the proton current density through the ACL thickness. Substituting (18) into Eq. (11), calculating the derivative and solving the resulting equation for η , we get the shape of overpotential through the ACL depth

$$\tilde{\eta}(\tilde{x}) = \ln\left(\frac{\varepsilon^2(\gamma^2 + \tilde{j}^2)}{1 - \varepsilon^2 \xi(\gamma^2 + \tilde{j}^2)}\right) \quad (22)$$

where $\tilde{j}(\tilde{x})$ is given by Eq. (18).

3.2 ACL polarization curve

Setting in (22) $\tilde{x} = 0$, we obtain the ACL polarization curve

$$\tilde{\eta}_0 = \ln\left(\varepsilon^2(\gamma^2 + \tilde{j}_0^2)\right) - \ln\left(1 - \varepsilon^2 \xi(\gamma^2 + \tilde{j}_0^2)\right) \quad (23)$$

Obviously, Eq. (23) fails to describe the overpotential at zero current, when the argument of the first logarithm tends to zero. This is the general defect of the Tafel equation, which stands behind Eq. (6).

By analogy to the Butler--Volmer equation, this defect can be corrected replacing the first logarithm in Eq. (23) by the arcsinh--function of the halved argument. Indeed, for $y > 2$ we have $\operatorname{arcsinh}(y) \cong \ln(2y)$, while for $y \ll 1$, $\operatorname{arcsinh}(y) \cong y$, which gives a correct asymptotics at small currents (zero overpotential at $j = 0$). With this, we get

$$\tilde{\eta}_0 = \operatorname{arcsinh}\left(\frac{\varepsilon^2}{2}(\gamma^2 + \tilde{j}_0^2)\right) - \ln\left(1 - \frac{\varepsilon^2(\gamma^2 + \tilde{j}_0^2)}{\tilde{i}_{ads}\tilde{c}_t}\right) \quad (24)$$

Here $\gamma(\tilde{j}_0)$ is given by Eq. (21) and we took into account Eqs. (14).

The first term in Eq. (24) is independent of the adsorption rate, which means that this term describes the activation overpotential for the electrochemical steps of MOR. Note that at large \tilde{j}_0 , this term exhibits doubling of the apparent Tafel slope, which is a well--known effect of poor proton transport in the ACL. Indeed, at $\tilde{j}_0 \gg 1$, $\gamma \rightarrow \pi$, hence γ can be neglected and the activation term reduces to

$$\tilde{\eta}_0^{act} = 2\ln(\varepsilon\tilde{j}_0) \quad (25)$$

which directly shows the Tafel slope doubling. At small overpotentials, $\gamma \cong \sqrt{2\tilde{j}_0}$, the term \tilde{j}_0^2 is small and the activation polarization reduces to

$$\tilde{\eta}_0^{act} = \operatorname{arcsinh}(\varepsilon^2\tilde{j}_0) \quad (26)$$

which is a standard Tafel law.

The second term in Eq. (24) has a form of a transport logarithm and it represents the overpotential required to bring methanol molecule to the catalyst surface. Though methanol adsorption is independent of overpotential, the electrochemical steps of MOR require methanol to be adsorbed on the catalyst surface, and the second term in Eq. (24) describes the respective quasi--transport voltage loss.

3.3 Half--cell polarization curve

Methanol concentration \tilde{c}_t in the ACL depends on the cell current density itself. A balance of methanol flux through the DMFC leads to the following relation between \tilde{c}_t and the methanol concentration in the feed channel \tilde{c}_h (Kulikovsky 2002)

$$\tilde{c}_t = (1 - \beta_*) \left(\tilde{c}_h - \frac{\tilde{j}_0}{j_{\text{lim}}^{\text{ref}}} \right) \quad (27)$$

where β_* is the crossover parameter

$$\beta_* = \frac{\beta}{1 + \beta}, \quad \beta = \frac{D_m l_b^a}{D_b^a l_m} \quad (28)$$

and

$$j_{\text{lim}}^{\text{ref}} = \frac{6FD_b^a c_{\text{ref}}}{l_b^a} \quad (29)$$

is the limiting current density due to the transport of reference methanol concentration in the ABL. Here D_b^a is the methanol diffusion coefficient in the ABL of a thickness l_b^a , D_m is the methanol diffusion coefficient in the membrane of a thickness l_m . Note that β_* varies in the range $0 < \beta_* < 1$; $\beta_* = 0$ corresponds to zero crossover, while $\beta_* \rightarrow 1$ describes the limit of fast rate of crossover. Estimates show that the typical value of β_* is between 0.2 and 0.4.

Substituting (27) into (24), we get

$$\tilde{\eta}_0 = \operatorname{arcsinh} \left(\frac{\varepsilon^2}{2} (\gamma^2 + \tilde{j}_0^2) \right) - \ln \left(1 - \frac{\varepsilon^2 (\gamma^2 + \tilde{j}_0^2)}{\tilde{i}_{\text{ads}}(1 - \beta_*) (\tilde{c}_h - \tilde{j}_0 / j_{\text{lim}}^{\text{ref}})} \right) \quad (30)$$

This is the general form of the half--cell polarization potential.

3.4 Limiting current density

The effective anode limiting current density \tilde{j}_{lim} is obtained if we equate the expression under the second logarithm in Eq. (30) to zero

$$\frac{\varepsilon^2 (\gamma^2 + \tilde{j}_0^2)}{\tilde{i}_{\text{ads}}(1 - \beta_*) (\tilde{c}_h - \tilde{j}_0 / j_{\text{lim}}^{\text{ref}})} = 1 \quad (31)$$

As γ is a rather complicated function of \tilde{j}_0 , Eq. (21), in the general case, Eq. (31) should be solved numerically. However, in the cases of small and large limiting currents, this equation can further be simplified.

3.4.1 Low limiting current: $\tilde{j}_{lim} \ll 1$

If $\tilde{j}_0 \ll 1$, we have $\gamma = \sqrt{2\tilde{j}_0}$ and the term \tilde{j}_0^2 in Eq. (31) can be omitted. Solving the resulting equation we find

$$\frac{1}{\tilde{j}_{lim}} = \frac{1}{\tilde{c}_h \tilde{j}_{lim}^{ref}} + \frac{1}{\tilde{i}_{ads}(1-\beta_*)\tilde{c}_h/(2\varepsilon^2)} \quad (32)$$

In the dimension variables this equation reads

$$\frac{1}{j_{lim}} = \frac{1}{j_{lim}^{ABL}} + \frac{1}{j_{lim}^{ads,low}} \quad (33)$$

where

$$j_{lim}^{ads,low} = \frac{l_t i_{ads}(1-\beta_*)c_h}{c_{ref}} \quad (34)$$

$$j_{lim}^{ABL} = \frac{6FD_b^a c_h}{l_b^a} \quad (35)$$

Here, $j_{lim}^{ads,low}$ is the low-current limiting current density due to the methanol adsorption on the catalyst surface, and j_{lim}^{ABL} is the limiting current due to the methanol transport in the ABL. Eq. (33) shows that the limiting currents corresponding to the two mechanisms of current limitation sum up as parallel resistivities.

Note that $j_{lim}^{ads,low}$ is proportional to the product of ACL thickness by the volumetric rate of methanol adsorption. In the low-current regime, the rate of MOR is uniformly distributed through the ACL, which leads to this simple proportionality.

3.4.2 High limiting current: $\tilde{j}_{lim}^2 \gg \pi^2$

In that case we can omit γ^2 in Eq.(31). Solving the resulting equation for \tilde{j}_0 , we get

$$\tilde{j}_{lim} = \sqrt{\left(\frac{\tilde{i}_{ads}(1-\beta_*)}{2\varepsilon^2 \tilde{j}_{lim}^{ref}}\right)^2 + \frac{\tilde{i}_{ads}(1-\beta_*)\tilde{c}_h}{\varepsilon^2} - \frac{\tilde{i}_{ads}(1-\beta_*)}{2\varepsilon^2 \tilde{j}_{lim}^{ref}}} \quad (36)$$

Eq. (36) can further be simplified to

$$\tilde{j}_{lim} = \begin{cases} \sqrt{\frac{\tilde{i}_{ads}(1-\beta_*)\tilde{c}_h}{\varepsilon^2}}, & 2\varepsilon^2 \tilde{j}_{lim}^{ref} / \tilde{i}_{ads} \gg 1 \\ \tilde{j}_{lim}^{ref} \tilde{c}_h, & 2\varepsilon^2 \tilde{j}_{lim}^{ref} / \tilde{i}_{ads} \ll 1 \end{cases} \quad (37)$$

In the dimension variables Eq. (37) reads

$$j_{\text{lim}} = \begin{cases} j_{\text{lim}}^{\text{ads,high}}, & j_{\text{lim}}^{\text{ref}} \gg l_t i_{\text{ads}} \\ j_{\text{lim}}^{\text{ABL}}, & j_{\text{lim}}^{\text{ref}} \ll l_t i_{\text{ads}} \end{cases} \quad (38)$$

where

$$j_{\text{lim}}^{\text{ads,high}} = \sqrt{2\sigma_t b i_{\text{ads}}(1 - \beta_*)c_h/c_{\text{ref}}} \quad (39)$$

is the high--current limiting current density due to the methanol adsorption on the catalyst surface. The limiting current due to methanol transport in the ABL $j_{\text{lim}}^{\text{ABL}}$ is still given by (35).

Note that $j_{\text{lim}}^{\text{ads,high}}$ is independent of the ACL thickness l_t , but it depends on the ACL proton conductivity σ_t and on the MOR Tafel slope b . In the case of high cell current, the electrochemical conversion runs near the membrane, in a thin *conversion domain* of a thickness in the order of $\sigma_t b/j_0$ (Kulikovsky 2010). This introduces an internal space scale to the problem, making it independent of the ACL thickness.

3.4.3 Remarks to Section 3.4

Equations of Section 3.4 show that there are three regimes of the anode operation. In the first regime, the anode performance is limited by the rate of methanol adsorption; this regime is realized if $j_{\text{lim}}^{\text{ref}} \gg l_t i_{\text{ads}}$. In the opposite limit of $j_{\text{lim}}^{\text{ref}} \ll l_t i_{\text{ads}}$, the anode current is limited by the rate of methanol diffusive transport in the ABL. The third regime is the mixed one: When $j_{\text{lim}}^{\text{ref}} \cong l_t i_{\text{ads}}$, both the mechanisms of current limitation affect the anode polarization curve and the effective limiting current density is given by Eq. (32) in the low--current regime, and by Eq. (36) in the high--current mode.

Comparison of Eqs. (39) and (35) suggests a means for distinguishing the mechanism of current limitation on the anode in the high--current mode. Indeed, $j_{\text{lim}}^{\text{ABL}}$ is independent of b and σ_t ; however, it depends on l_b^a . On the other hand, $j_{\text{lim}}^{\text{ads,high}}$ is independent of l_b^a , but it depends on b and σ_t . Changing b or σ_t is difficult; however, changing l_b^a is relatively simple by taking the anode backing media of different thickness. Thus, preparing MEAs with the different ABL thicknesses could help to understand the origin of current limitation.

4. Results and discussion

The quality of Eq. (24) can be checked by comparison of this equation to the exact numerical polarization curve, which follows from the direct solution of the system (11), (12). For the sake of comparison we assume zero transport loss in the ABL and zero crossover; hence, in Eq. (24), we set $\tilde{c}_t = 1$. Fig. 2 shows that the analytical curve works well up to the limiting current density. Further numerical tests show that Eq. (24) only fails in a small vicinity of the adsorption--limiting current (Fig. 2). Note, however, that the analytical curve gives quite an accurate value of the limiting current density, while the exact value of overpotential in this region is usually of limited interest.

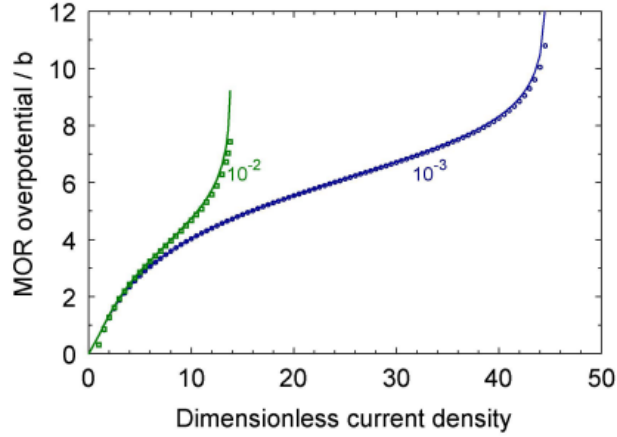


Fig. 2 Exact numerical (points) and analytical (lines, Eq. (24)) polarization curves of the anode catalyst layer for the indicated values of parameter ξ . In both the cases, parameter $\varepsilon = 1$

Nordlund and Lindbergh (2004) published a set of measured polarization curves of DMFC anode. Eq. (24) has been fitted to their data and the results are shown in Fig. 3. In the paper of Nordlund and Lindbergh, the thickness and porosity of the anode backing layer have not been specified and we assume that the voltage loss due to methanol transport in the backing layer is small. For simplicity, we also neglect the crossover by setting $\beta_* = 0$; thus, in Eq. (24) we set $\tilde{c}_t = \tilde{c}_h$. All the experimental curves exhibit constant shift along the η -axis. This shift, which presumably is due to the oxygen crossover through the membrane has been taken into account by adding a constant $\eta_* = 0.11$ V to the dimensional form of Eq. (24). The curves have first been fitted using the NonlinearFit procedure of Maple[®], and finally fine tuning of the fitting parameters has been performed, in order to maximize a number of common parameters between the curves.

Fig. 3 shows the experimental and model curves for the two cell temperatures (50 °C and 70 °C) and the indicated methanol molar concentrations. The fitting parameters are listed in Table 1. As can be seen, all the parameters except i_* and $\tilde{i}_{ads} = i_{ads}/i_*$ were kept fixed, while i_* was taken to be constant for each temperature and \tilde{i}_{ads} was varied to get a best fit for every methanol concentration. The plots of resulting \tilde{i}_{ads} as a function of normalized methanol concentration c_h/c_{ref} are shown in Fig. 4. These plots are linear, which suggests that the adsorption rate constant i_{ads} is itself linear in methanol concentration (Fig. 4), i.e., the rate of methanol adsorption is quadratic in \tilde{c}_h . The reason for that is unclear.

Overall, the quality of fitting is reasonably good, taking into account that with the data in Fig. 4, at a fixed cell temperature, parameters for all the curves are the same. However, for different types of catalysts these parameters may differ, so that the predicting capability of Eq. (24) should not be overestimated.

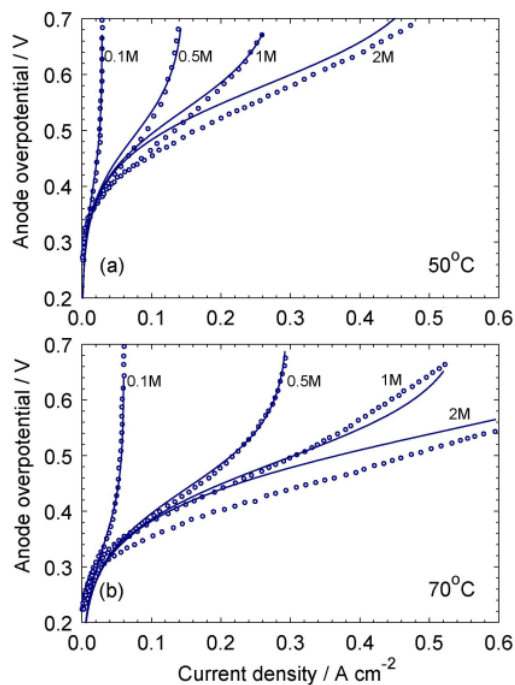


Fig. 3 Our analytical (lines) and experimental polarization curves of DMFC anode measured by Nordlund and Lindbergh (2004) for the indicated methanol concentrations and cell temperature of (a) 50 °C and (b) 70 °C. The fitting parameters are listed in Table 1

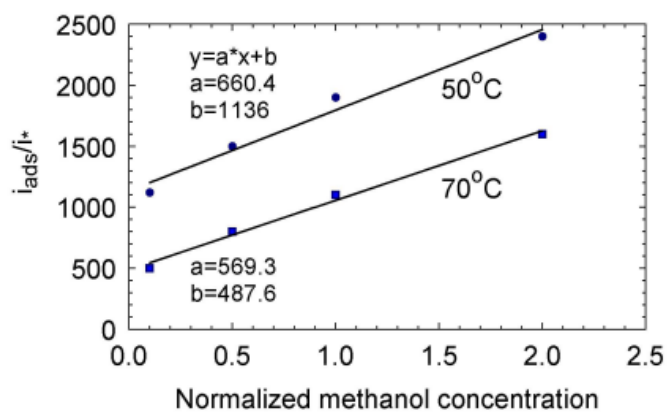


Fig. 4 Dependence of parameter \tilde{i}_{ads} on the normalized methanol concentration for the two cell temperatures of 50 °C and 70 °C. Linear fits are also displayed

Table 1 Fitting parameters for the curves in Figure 3. Note that due to the small ACL thickness, in both the cases $\varepsilon \cong 10$. For a typical 100 μm -thick ACL this parameter is in the order of unity. The layer proton conductivity σ_t is taken from Havranek and Wippermann (2004)

	70 °C	50 °C
b , V		0.06
l_b^a , cm		0.02
l_t , cm		0.0014
σ_t , $\Omega^{-1} \text{ cm}^{-1}$		0.003
D_b^a , $\text{cm}^2 \text{ s}^{-1}$		$8 \cdot 10^{-3}$
η_* , V		0.11
j_* , A cm^{-2}		0.129
i_* , A cm^{-3}	1.0	0.2
ε	11.98	15.15
	$\tilde{i}_{ads} \equiv i_{ads}/i_*$	$\tilde{i}_{ads} \equiv i_{ads}/i_*$
(0.1M)	500	1120
(0.5M)	800	1500
(1.0M)	1100	1900
(2.0M)	1600	2400

Nordlund and Lindbergh (2004) suggested a simple analytical polarization curve. In our notations, a kinetic part of their polarization equation (not accounting for the methanol transport in the ABL) has the form

$$j_0 = \frac{j_* \exp(\eta_0/b)}{1 + \xi \exp(\eta_0/b)} \quad (40)$$

where $\eta_0 = E_* - E_c$, E_c is the electrode potential, and E_* , j_* , and ξ are the fitting parameters. Solving (40) for η_0 , we get the polarization curve

$$\eta_0 = \ln\left(\frac{j_0}{j_*}\right) - \ln\left(1 - \frac{\xi j_0}{j_*}\right) \quad (41)$$

This equation differs from Eq. (24) by the absence of terms quadratic in j_0 . Physically, this means that Eq. (41) ignores the proton transport loss in the ACL.

In other words, Eq. (41) is justified provided that the ACL proton conductivity is large. In that case, the rate of MOR is nearly uniform across the ACL and the total current produced by MOR is simply a product of the reaction rate (6) by the ACL thickness, which eventually leads to Eqs. (40) and (41).

According to the model above, in experiments of Nordlund and Lindbergh, the approximation of ideal proton transport is justified for currents below 100 mA cm^{-2} . To show this explicitly, we plot the model shape of MOR rate along x . By definition, $\tilde{R}_{MOR} = -\partial\tilde{j}/\partial\tilde{x}$; using here (11), we get

$$\tilde{R}_{MOR} = \frac{\gamma^2 + j^2}{2} \quad (42)$$

where $\tilde{j}(\tilde{x})$ is given by (11) and γ is given by (21).

Fig. 5(a) shows the MOR rate through the ACL thickness for the one-molar methanol concentration and the current densities of 100, 200 and 300 mA cm^{-2} . Fig. 5(b) depicts the respective shapes of the proton current density and of the local overpotential η . Parameters for these plots result from fitting of the polarization curves corresponding to 70°C (Table 1).

As can be seen, even in a $14\text{-}\mu\text{m}$ ACL used by Nordlund and Lindbergh, for the currents above 200 mA cm^{-2} , R_{MOR} and overpotential are far from being uniform. Note that for the thicker layers, quite a substantial non-uniformity is achieved at lower currents. Physically, poor proton transport in the ACL forces the reaction to run faster at the membrane interface, where protons are “cheaper” (see (Kulikovsky 2010) for discussion).

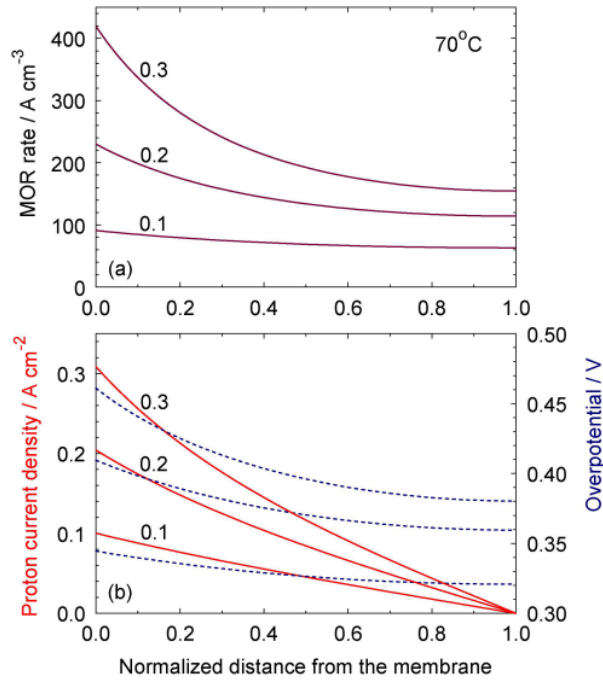


Fig. 5 The model shapes of (a) the MOR rate and (b) the proton current density and local MOR overpotential through the catalyst layer thickness for the indicated mean cell current density. Cell temperature is 70°C ; parameters for the calculations are taken from the curve fitting in Fig. 3

5. Conclusions

We report a model for the DMFC anode performance. The model takes into account poor proton transport in the anode catalyst layer, methanol transport in the anode backing layer, methanol crossover through the membrane, and a two-step kinetics of methanol oxidation reaction (MOR), which includes the potential-independent step of methanol adsorption on the catalyst surface. A simple analytical equation for the half-cell overpotential is derived. Analysis of this equation leads to analytical expressions for the limiting current densities of the anode. The current can be limited either by the rate of methanol adsorption, or by the rate of methanol transport in the backing layer.

The model equation is fitted to the experimental anode polarization curves measured by Nordlund and Lindbergh. For each cell temperature, a set of common fitting parameters reasonably well describes the curves measured for various methanol concentrations.

References

- Argyropoulos, P., Scott, K., Shukla, A.K. and Jackson, C. (2002), "Empirical model equations for the direct methanol fuel cell", *Fuel Cells*, **2**(2), 78-82.
- Arisetty, S., Krewer, U., Advani, S.G. and Prasada, A.K. (2010), "Coupling of kinetic and mass transfer processes in direct methanol fuel cells", *J. Electrochem. Soc.*, **157**(10), B1443-B1455.
- Bagotzky, V.S. and Vasilyev, Y.B. (1964), "Some characteristics of oxidation reactions of organic compounds of platinum electrodes", *Electrochim. Acta*, **9**(7), 869-882.
- Bagotzky, V. S. and Vasilyev, Y. B. (1967), "Mechanism of electrooxidation of methanol on the platinum electrodes", *Electrochim. Acta*, **12**(9), 1323-1343.
- Baldaus, M. and Preidel, W. (2001), "Experimental results on the electrochemical oxidation of methanol in PEM fuel cells", *J. Appl. Electrochem.*, **31**(7), 781-786.
- Baxter, S.F., Battaglia, V.S. and White, R.E. (1999), "Methanol fuel cell model: Anode", *J. Electrochem. Soc.*, **146**(2), 437-47.
- Casalegno, A. and Marchesi, R. (2008), "DMFC anode polarization: Experimental analysis and model validation", *J. Power Sources*, **175**(1), 372-382.
- Cho, C., Kim, Y. and Chang, Y.S. (2009), "Performance analysis of direct methanol fuel cell for optimal operation", *J. Therm. Sci. Techn.*, **4**(3), 414-423.
- Divisek, J., Fuhrmann, J., Gärtner, K. and Jung, R. (2003), "Performance modeling of a direct methanol fuel cell", *J. Electrochem. Soc.*, **150**(6), A811-A825.
- Dohle, H., Divisek, J. and Jung, R. (2000), "Process engineering of the direct methanol fuel cell", *J. Power Sources*, **86**(1-2), 469-477.
- Gasteiger, H.A., Markovic', N., P.N. Ross, J. and Cairns, E.J. (1993), "Methanol electrooxidation on well-characterized Pt-Ru alloys", *J. Phys. Chem.*, **97**(46), 12020-12029.
- Havranek, A. and Wippermann, K. (2004), "Determination of proton conductivity in anode catalyst layers in direct methanol fuel cell (DMFC)", *J. Electroanal. Chem.*, **567**(2), 305-351.
- Jeng, K.T. and Chen, C.W. (2002), "Modeling and simulation of a direct methanol fuel cell anode", *J. Power Sources*, **112**(2), 367-375.
- Jiang, J. and Kucernak, A. (2005), "Solid polymer electrolyte membrane composite microelectrode investigations of fuel cell reactions. II: Voltammetric study of methanol oxidation at the nanostructured platinum microelectrode|Nafion[®] membrane interface", *J. Electroanal. Chem.*, **576**, 223-236.
- Ko, D.H., Lee, M., Jang, W.H. and Krewer, U. (2008), "Non-isothermal dynamic modelling and optimization of a direct methanol fuel cell", *J. Power Sources*, **180**(1), 71-83.
- Krewer, U., Christov, M., Vidakovic, T. and Sundmacher, K. (2006), "Impedance spectroscopic analysis of the electrochemical methanol oxidation kinetics", *J. Electroanal. Chem.*, **589**(1), 148-159.

- Krewer, U., Yoon, H.K. and Kim, H.T. (2008), "Basic model for membrane electrode assembly design for direct methanol fuel cells", *J. Power Sources*, **175**(2), 760-772.
- Kulikovsky, A.A. (2002), "The voltage current curve of a direct methanol fuel cell: "exact" and fitting equations", *Electrochem. Comm.*, **4**(12), 939-946.
- Kulikovsky, A.A. (2003), "Analytical model of the anode side of DMFC: Effect of non-Tafel kinetics on cell performance", *Electrochem. Comm.*, **5**(7), 530-538.
- Kulikovsky, A.A. (2005), "Active layer of variable thickness: The limiting regime of anode catalyst layer operation in a DMFC", *Electrochem. Comm.*, **7**(10), 969-975.
- Kulikovsky, A.A. (2010), "The regimes of catalyst layer operation in a fuel cell", *Electrochim. Acta*, **55**(22), 6391-6401.
- Kulikovsky, A.A. (2012), "Catalyst layer performance in PEM fuel cell: analytical solutions", *Electrocatalysis*, **3**(2), 132-138.
- Lam, A., Wetton, B. and Wilkinson, D.P. (2011), "One-dimensional model for a direct methanol fuel cell with a 3D anode structure", *J. Electrochem. Soc.*, **158**(1), B29-B35.
- Lamy, C. and Leger, J.M. (1991), "Electrocatalytic oxidation of small organic molecules at platinum single crystals", *J. Chimie Physique*, **88**, 1649-1671.
- Meyers, J. and Newman, J. (2002), "Simulation of the direct methanol fuel cell. II. modeling and data analysis of transport and kinetic phenomena", *J. Electrochem. Soc.*, **149**(6), A718-A728.
- Miao, Z., He, Y.L., Li, X.L. and Zou, J.Q. (2008), "A two-dimensional two-phase mass transport model for direct methanol fuel cells adopting a modified agglomerate approach", *J. Power Sources*, **185**(2), 1233-1246.
- Murgia, G., Pisani, L., Shukla, A.K. and Scott, K. (2003), "A numerical model of a liquid-feed solid polymer electrolyte DMFC and its experimental validation", *J. Electrochem. Soc.*, **150**(9), A1231-A1245.
- Nordlund, J. and Lindbergh, G. (2004), "Temperature-dependent kinetics of the anode in the DMFC", *J. Electrochem. Soc.*, **151**(9), A1357-A1362.
- Petry, O.A., Podlovchenko, B.I., Frumkin, A.N. and Lal, H. (1965), "The behaviour of platinized-platinum and platinum-ruthenium electrodes in methanol solutions", *J. Electroanal. Chem.*, **10**(4), 253-269.
- Scott, K., Taama, W.M., Kramer, S., Argyropoulos, P. and Sundmacher, K. (1999), "Limiting current behaviour of the direct methanol fuel cell", *Electrochimica Acta*, **45**(6), 945-957.
- Tarasevich, M.R., Sadkowsky, A. and Yeager, E. (1983), *Oxygen electrochemistry*, (Eds, Coway, B.E., Bockris, J.O., Yeager, E., Khan, S.U.M. and White, R.E.), *Comprehensive Treatise of Electrochemistry*, **7**, 310-398. Plenum Press, New-York.
- Xu, C., He, Y. L., Zhao, T. S., Chen, R., and Ye, Q. (2006), "Analysis of mass transport of methanol at the anode of a direct methanol fuel cell", *J. Electrochem. Soc.*, **153**, A1358-A1364.
- Yang, W. W. and Zhao, T. S. (2007), "A two-dimensional, two-phase mass transport model for liquid-feed DMFCs", *Electrochimica Acta*, **52**, 6125-6140.
- Zhao, T. S., Xu, C., Chen, R., and Yang, W. W. (2009), "Mass transport phenomena in direct methanol fuel cells", *Progress in Energy and Combustion Sci.*, **35**, 275-292.

Nomenclature

\sim	Marks dimensionless variables
b	MOR Tafel slope (V)
c_t	Methanol molar concentration in the catalyst layer (mol cm^{-3})
c_h	Methanol molar concentration in the anode channel (mol cm^{-3})
c_{ref}	Reference methanol molar concentration (mol cm^{-3})
D_b^a	Methanol diffusion coefficient in the ABL ($\text{cm}^2 \text{ s}^{-1}$)
D_m	Methanol diffusion coefficient in the membrane ($\text{cm}^2 \text{ s}^{-1}$)
E_c	Electrode potential (V)
F	Faraday constant
j	Local proton current density (A cm^{-2})
j_0	Cell current density (A cm^{-2})
j_*	Characteristic current density $\sigma_t b/l_t$, (A cm^{-2})
j_{lim}^{ref}	Reference limiting current density (A cm^{-2}), Eq. (29)
j_{lim}^{ABL}	Limiting current density due to methanol transport in the anode backing layer (A cm^{-2}), Eq. (35)
$j_{lim}^{ads,low}$	Low--current limiting current density due to methanol adsorption on the catalyst surface (A cm^{-2}), Eq. (34)
$j_{lim}^{ads,high}$	High--current limiting current density due to methanol adsorption on the catalyst surface (A cm^{-2}), Eq. (39)
i_*	MOR volumetric exchange current density (A cm^{-3})
i_{ads}	Equivalent volumetric rate of methanol adsorption (A cm^{-3})
l_b^a	Anode backing layer thickness (cm)
l_m	Membrane thickness (cm)
l_t	Catalyst layer thickness (cm)
R_{MOR}	Volumetric MOR rate (A cm^{-3})
T	Cell temperature (K)
x	Coordinate through the ACL (cm)

Superscripts

<i>a</i>	Anode
<i>ads</i>	Methanol adsorption
<i>ABL</i>	Anode backing layer
<i>ref</i>	Reference value
0	Inlet

Subscripts

*	Marks fitting parameter
<i>ads</i>	Methanol adsorption
<i>b</i>	Backing layer
<i>h</i>	Channel
lim	Limiting
<i>MOR</i>	Methanol oxidation reaction
<i>m</i>	Membrane
<i>ref</i>	Reference value
<i>t</i>	Catalyst layer

Greek

β	Dimensionless crossover parameter, (28)
β_*	$\beta/(1 + \beta)$
γ	Dimensionless parameter, (21)
η	Local overpotential (V)
η_0	Total voltage loss (half-cell overpotential) (V)
η_*	Constant shift of polarization curve (V)
ε	Dimensionless reaction penetration depth, (13)
σ_t	Catalyst layer ionic conductivity ($\Omega^{-1} \text{ cm}^{-1}$)
ξ	Inverse dimensionless rate of MeOH adsorption, (14)